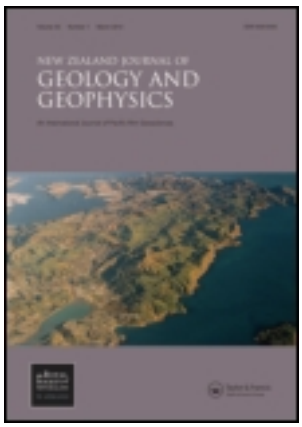

New Zealand Journal of Geology and Geophysics
Publication details, including instructions for authors and subscription information:
http://www.tandfonline.com/loi/tnzg20

Methane seepage and its relation to slumping and gas hydrate at the Hikurangi margin, New Zealand

Kevin Faure [a], Jens Greinert [b c], Ingo A. Pecher [c], Ian J. Graham [c], Gary J. Massoth [c], Cornel E. J. de Ronde [c], Ian C. Wright [d], Edward T. Baker [e] & Eric J. Olson [f]

[a] National Isotope Centre, GNS Science, PO Box 31312, Lower Hutt, 5040, New Zealand
E-mail:

[b] Renard Centre of Marine Geology (RCMG), Ghent University, Krijgslaan 281 s.8, Gent, B-9000, Belgium

[c] GNS Science, PO Box 30368, Lower Hutt, 5040, New Zealand

[d] National Institute of Water and Atmospheric Research, PO Box 14901, Wellington, 6241, New Zealand

[e] NOAA/PMEL, 7600 Sand Point Way NE, Seattle, WA, 98115-0070, USA

[f] School of Oceanography, University of Washington, Seattle, WA, 98195, USA

Published online: 22 Sep 2010.

To cite this article: Kevin Faure , Jens Greinert , Ingo A. Pecher , Ian J. Graham , Gary J. Massoth , Cornel E. J. de Ronde , Ian C. Wright , Edward T. Baker & Eric J. Olson (2006): Methane seepage and its relation to slumping and gas hydrate at the Hikurangi margin, New Zealand, New Zealand Journal of Geology and Geophysics, 49:4, 503-516

To link to this article: http://dx.doi.org/10.1080/00288306.2006.9515184

New Zealand Journal of Geology & Geophysics, 2006, Vol. 49: 503–516
0028–8306/06/4904–0503

Methane seepage and its relation to slumping and gas hydrate at the Hikurangi margin, New Zealand

KEVIN FAURE[1]
JENS GREINERT[2,3]
INGO A. PECHER[3]
IAN J. GRAHAM[3]
GARY J. MASSOTH[3]
CORNEL E. J. DE RONDE[3]
IAN C. WRIGHT[4]
EDWARD T. BAKER[5]
ERIC J. OLSON[6]

[1]GNS Science
National Isotope Centre
PO Box 31312
Lower Hutt 5040, New Zealand
k.faure@gns.cri.nz

[2]Renard Centre of Marine Geology (RCMG)
Ghent University
Krijgslaan 281 s.8
B-9000 Gent, Belgium

[3]GNS Science
PO Box 30368
Lower Hutt 5040, New Zealand

[4]National Institute of Water and Atmospheric Research
PO Box 14901
Wellington 6241, New Zealand

[5]NOAA/PMEL
7600 Sand Point Way NE
Seattle WA 98115-0070, USA

[6]School of Oceanography
University of Washington
Seattle WA 98195, USA

Abstract Dissolved methane and high resolution bathymetry surveys were conducted over the Rock Garden region of Ritchie Ridge, along the Hikurangi margin, eastern New Zealand. Multibeam bathymetry reveals two prominent, northeast trending ridges, parallel to subduction along the margin, that are steep sided and extensively slumped. Elevated concentrations of methane (up to 10 nM, 10× background) within the water column are associated with a slump structure at the southern end of Eastern Rock Garden. The anomalous methane concentrations were detected by a methane sensor (METS) attached to a conductivity-temperature-depth-optical backscatter device (CTDO) and are associated with elevated light scattering and flare-shaped backscatter signals revealed by the ship's echo sounder. Increased particulate matter in the water column, possibly related to the seepage and/or higher rates of erosion near slump structures, is considered to be the cause of the increased light scattering, rather than bubbles in the water column. Methane concentrations calculated from the METS are in good agreement with concentrations measured by gas chromatography in water samples collected at the same time. However, there is a c. 20 min (c. 900 m) delay in the METS signal reaching maximum CH_4 concentrations. The maximum methane concentration occurs near the plateau of Eastern Rock Garden close to the edge of a slump, at 610 m below sea level (mbsl). This is close to the depth (c. 630 mbsl) where a bottom simulating reflector (BSR) pinches out at the seafloor. Fluctuating water temperatures observed in previous studies indicate that the stability zone for pure methane hydrate in the ocean varies between 630 and 710 mbsl. However, based on calculations of the geothermal gradients from BSRs, we suggest gas hydrate in the study area to be more stable than hydrate from pure methane in sea water, moving the phase boundary in the ocean upward. Small fractions of additional higher order hydrocarbon gases are the most likely cause for increased hydrate stability. Relatively high methane concentrations have been measured down to c. 1000 mbsl, most likely in response to sediment slumping caused by gas hydrate destabilisation of the sediments and/or marking seepage through the gas hydrate zone.

Keywords Hikurangi margin; Ritchie Ridge; methane; hydrate; multibeam bathymetry; slumping

INTRODUCTION

Anoxic marine sediments are a major source of methane (CH_4) produced by bacteria that in the marine environment consume hydrogen and carbon dioxide (Whiticar 1999). Upward migrating pore water transports CH_4-rich fluids which are expelled at cold seeps. Cold seeps are common in sediments deposited at polar continental shelves and active and passive continental margins (Kvenvolden 1988; Jørgensen 1992; Paull et al. 1995; Orpin 1997; Suess et al. 1999, Naudts et al. 2006). In addition, methane enrichment in sea water, together with heat, Fe, Mn, and ^3He enrichment, are well known indicators for seafloor hydrothermal activity, because hydrothermal fluids are highly enriched in these compounds relative to background sea water (Lilley et al. 1995). Geochemical surveying of CH_4 in the water column is a common method for locating active seep or vent sites and for monitoring fluid activity. However, CH_4 is diluted very rapidly, distributed by currents, and is actively consumed in oxygenated sea water. Thus, elevated CH_4 concentrations around seeps are usually only a temporal "snapshot", as shown by water sampling at the same site within a few hours that can produce very different results (e.g., Heeschen et al. 2005). Even if the flow of CH_4 from deeper sediment horizons increases, the CH_4 into the water column may not similarly follow, as the anaerobic oxidation of CH_4 via sulfate reduction (AOM, e.g., Boetius et

G06014; Online publication date 30 November 2006
Received 16 June 2006; accepted 24 November 2006

al. 2000) builds a very efficient filter for CH_4 discharge into the water column (Sommer et al. 2006) by inducing carbonate precipitation (Kulm et al. 1986; Ritger et al. 1987; Greinert et al. 2001) and enhancing the microbial turnover rate (Nauhaus et al. 2002; Treude et al. 2003). Approximately 90% of the CH_4 is recycled through bacterially driven anaerobic oxidation processes such that marine environments contribute only 2% of the annual CH_4 flux to the atmosphere (Reeburgh 1996).

Studies of cold seeps over the past two decades have shown that high CH_4 concentrations are often associated with gas hydrate deposits (e.g., Borowski et al. 1997; Suess et al. 1999, Bohrmann et al. 2003; Milkov 2005). Gas hydrates are solid clathrate compounds with a crystalline structure hosting low molecular weight gases, such as CH_4, within cubic or hexagonal water cages. Hydrates form at low temperature and high pressure in seafloor sediments if the CH_4 concentration is sufficiently high (above or close to saturation) for nucleation (Kvenvolden 1988, 1998). Gas hydrates are increasingly important because they represent both a potentially major exploitable energy source (Kvenvolden 1988, 1993; Collett & Kuuskraa 1998) and have implications for the global carbon-cycle (Buffett & Archer 2004). These factors, and the potential of gas hydrates as a geo-hazard (the linkage between gas hydrate decomposition and weakening of seafloor stability), is the driving force behind gas hydrate research.

In September 2004, a multibeam and geochemical survey of the water column was undertaken in the Rock Garden area of Ritchie Ridge, along the Hikurangi margin, on the east coast of New Zealand's North Island (Fig. 1). It was the first geochemical gas hydrate survey of the water column undertaken in New Zealand waters. The Hikurangi margin is known for the occurrence of a widespread, strong bottom simulating reflection (BSR) seen in seismic data (e.g., Henrys et al. 2003) and indications of active CH_4 seepage (Lewis & Marshall 1996). The aims of the survey were: (1) to get detailed morphological information of the seafloor; (2) to confirm the existence of a hydroacoustic plume in the water column in the Rock Garden region as reported by Lewis & Marshall (1996); (3) to map the CH_4 distribution by CTDO-tows with discrete water sampling and continuous data logging of a METS methane sensor; and (4) to evaluate whether there is a relationship between submarine slump structures and the gas hydrate stability zone that could be a possible cause of methane release.

STUDY AREA

The Hikurangi margin forms as a compressional accretionary prism with oblique subduction of the Pacific plate beneath the Australian plate (Fig. 1 inset). Subduction started at c. 21 Ma, forming a large accretionary prism that is partially exposed onshore (Field et al. 1997). The study area, informally named the Rock Garden by local fisherman, is the southern termination of Ritchie Ridge (Fig. 1). The origin of Rock Garden's uplift is not well understood, although it may be caused by either thrusting associated with subduction or subduction of a seamount (Pecher et al. 2003). Based on crustal seismic data, it is interpreted that older material of unknown age is being exhumed at Rock Garden's crests (Pecher et al. 2005).

The first reports of active, or relatively recent, fluid seepage of CH_4 and H_2S-rich fluids from Rock Garden were made in 1994 by fishermen who obtained live specimens of seep-associated fauna from the New Zealand region—a *Bathymodiolus*-like mussel. They also observed a "plume" in the water column with a single beam echo sounder (Lewis & Marshall 1996; vent site number LM-3, Fig. 2). Although Lewis and Marshall did not explicitly conclude that this "plume" is caused by rising (methane) bubbles, this is the most likely explanation. Here, we will refer to hydroacoustic "plumes" as flares (Greinert et al. 2006; Naudts et al. 2006) to distinguish them from geochemical plumes. Subsequent sampling of the site obtained clams of the genus *Calyptogena* and again detected a flare rising 250 m above the seabed that mushroomed out within the water column at 650 mbsl (Lewis & Marshall 1996). Dredge sampling recovered carbonates associated with the chemoautotrophic fauna. Carbon isotope values of the calcitic and dolomitic carbonate cement indicate a thermogenic CH_4 source for the carbonate (Lewis & Marshall 1996). Two other flares were observed by fishermen and during high-resolution seismic surveys—LM-9 at 1140 mbsl and LM-10 at 725 mbsl (see Fig. 1)—but dredging at both sites failed to retrieve any seep-associated fauna (Lewis & Marshall 1996). The four seep-related sites (LM-1, LM-3, LM-9, LM-10; Fig. 1) distributed over a length of 260 km along the Hikurangi margin indicate that CH_4-rich seeps may be more common than presently known, especially if the widespread presence of BSR along the Hikurangi margin (Katz 1982; Townend 1997; Henrys et al. 2003) is accepted. Before this study, gas hydrate or CH_4-venting related geochemical data had not been acquired in New Zealand. Thus, the verification of the presence of gas hydrates and their gas composition, as well as the composition of the hydroacoustically observed bubbles and expelling fluids, still has to be addressed.

In the Rock Garden region, where the seafloor is relatively flat (575–790 mbsl), gas hydrate is predicted to be stable along much of the ridge, dependent on temperature and composition of the gas (Pecher et al. 2004). Seismic data across the eastern Rock Garden indicate that submarine erosion is occurring near the top of gas hydrate stability, as marked by BSR pinchouts (c. 600 mbsl) at the edge of a plateau-like crest (Fig. 3). Pecher et al. (2005) interpret that seafloor erosion above the gas hydrate stability zone results from a combination of two mechanisms. Firstly, depressurisation during uplift results in an upward movement of the base of gas hydrate stability relative to the seafloor, leading to gas hydrate dissociation, net pore volume expansion, and subsequently overpressure at the base of the gas hydrate stability zone. This overpressure is predicted to cause slumps close to the top of gas hydrate stability, as observed in seismic (Fig. 3) and bathymetric data. Secondly, temperature fluctuations of at least 0.9°C (Pecher et al. 2005) may lead to repeated formation and dissociation of gas hydrates close to the seafloor, leading to repeated pore volume expansion and contraction, weakening the seafloor in a frost-heave-like mechanism. The focusing of upward migrating fluids results in a sufficient supply of CH_4 to form a free gas phase, and thereby initiates gas hydrate formation. The seismic reflection data presented by Pecher et al. (2004), which show conduit-like zones supplying gas towards the seafloor, supports this contention.

The background CH_4 concentrations for the water column are unknown because no dissolved CH_4 data exist for Rock Garden or anywhere else in New Zealand. In this case, the Rock Garden CH_4 profiles are compared with CH_4 concentrations determined from three casts, deployed some distance from known seep sites, during the same expedition along the Kermadec arc, c. 800 km to the north. These are the only comparative data from the New Zealand region at

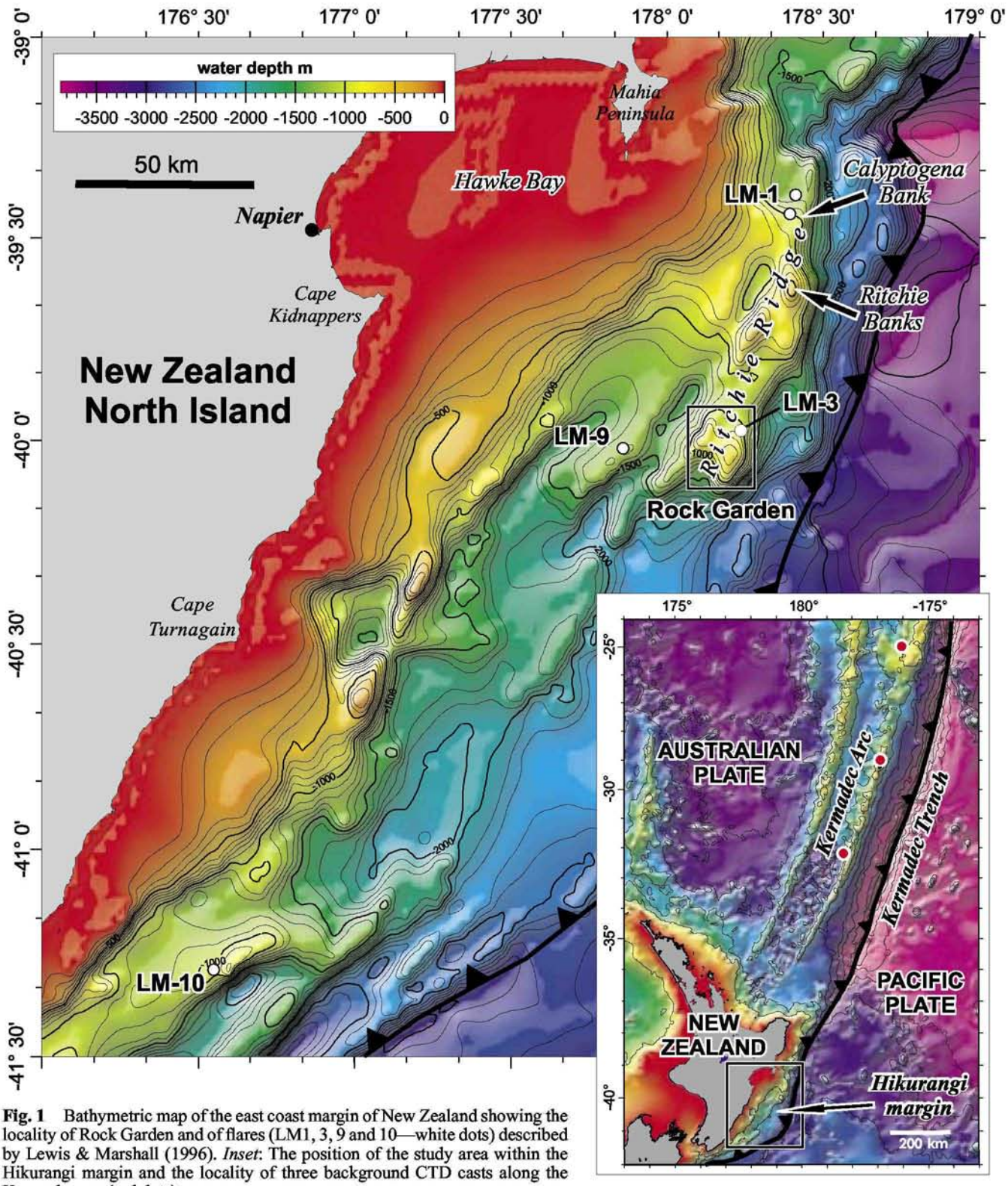

Fig. 1 Bathymetric map of the east coast margin of New Zealand showing the locality of Rock Garden and of flares (LM1, 3, 9 and 10—white dots) described by Lewis & Marshall (1996). *Inset*: The position of the study area within the Hikurangi margin and the locality of three background CTD casts along the Kermadec arc (red dots).

a distance from hydrothermal vent sources (see Fig. 1 for cast locations). In our survey, a vertical cast (V04D-01) was deployed c. 10 km southeast of Rock Garden to obtain a CH_4 background profile (Fig. 2). Two horizontal CTDO-tows (T04D-01 and T04D-02) were undertaken to survey the plateau and the northeast and southwest edges of the western and eastern Rock Garden, respectively. One of the tows (T04D-02) crossed the locality of the flare described by Lewis & Marshall (1996; LM-3 in Fig. 2). A second vertical cast (V04D-02) on the eastern Rock Garden was undertaken after high CH_4 concentrations were detected by the METS sensor in tow T04D-02 (Fig. 2).

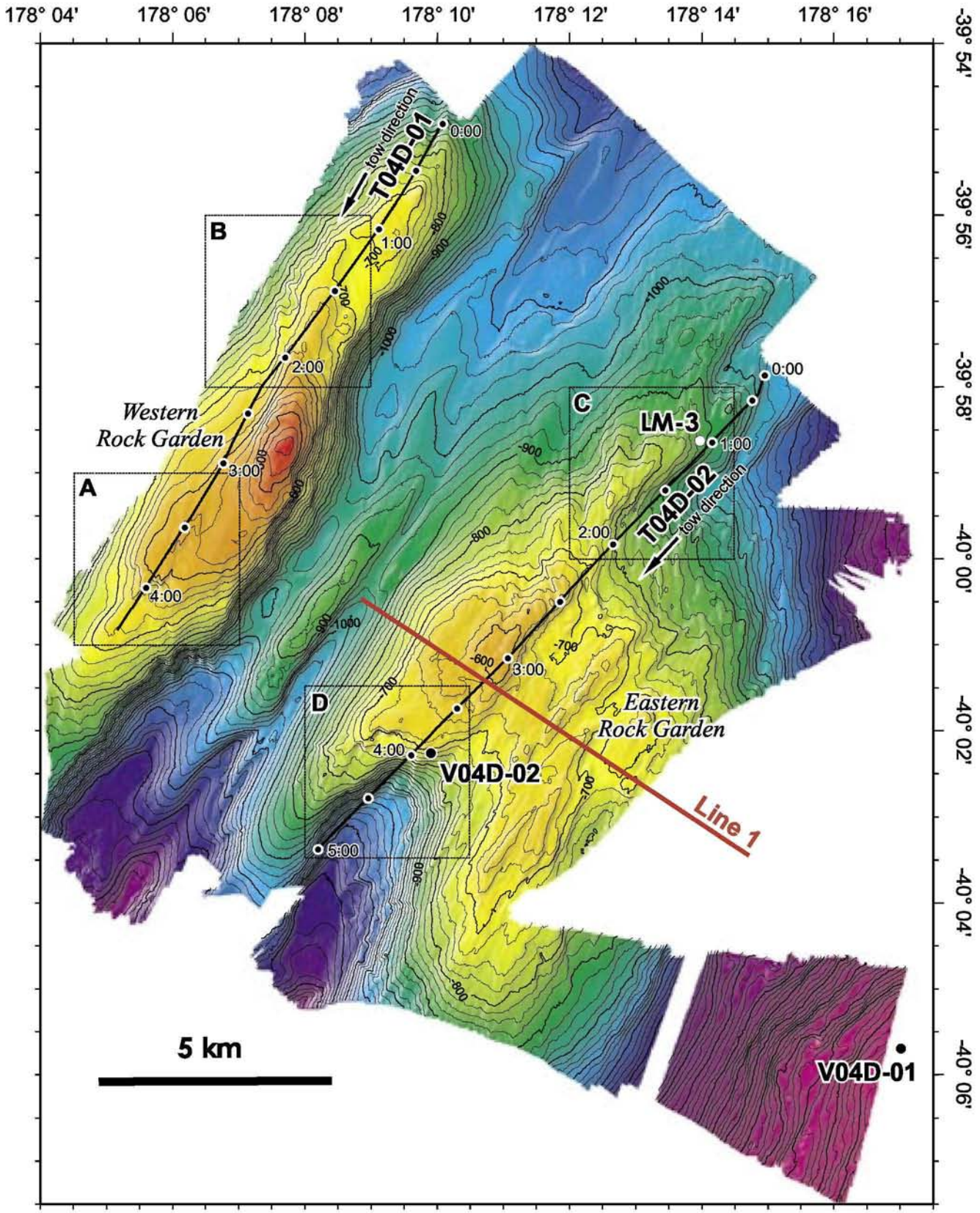

Fig. 2 Bathymetric map of the Rock Garden region showing the location of CTD tow deployments (T04D-01 and T04D-02) and vertical CTD casts (V04D-01 and V04D-02). Tow directions are shown and hourly time lapses indicated on tow lines. Line 1 (red) is the approximate position of the seismic profile shown in Fig. 3. Detailed bathymetry within blocks A, B, C and D is shown in Fig. 4.

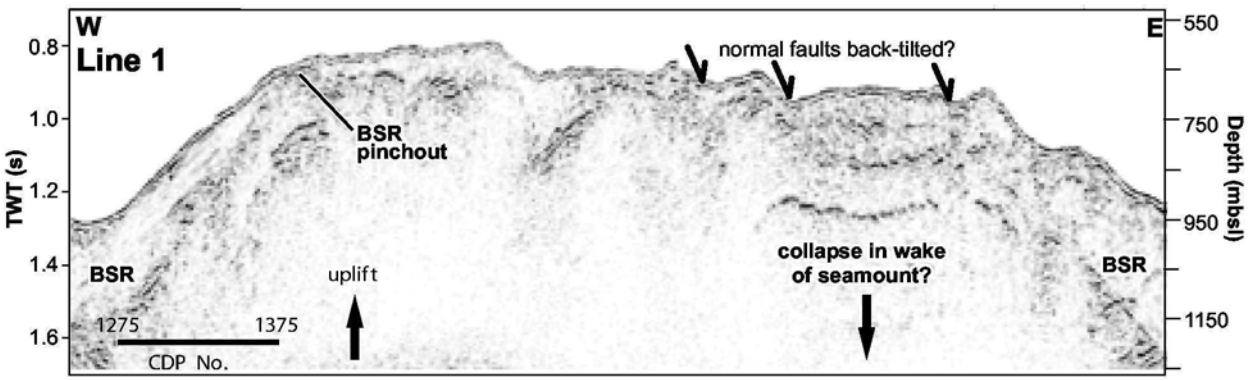

Fig. 3 Seismic profile from Eastern Rock Garden (after Pecher et al. 2005)—see Fig. 2. The location of clearly identified BSR reflections is shown, as well as where the BSR appears to pinch out at the edges of plateau. The BSR pinchout occurs at 0.84 ± 0.02 s corresponding to 630 ± 20 m, using a water velocity from seismic velocity analysis of 1500 ± 10 m/s. The approximate depth calculated for gas hydrate stability ranges between 630 and 710 mbsl, assuming pure methane in sea water, compared to 570 and 645 using the gas composition in Pecher et al. (2005) (see text). The location of the Common Depth Point numbers (CDP no.) are indicated in the bottom left hand corner.

METHODS

Multibeam mapping was undertaken with an EM300 system (30 kHz) installed on the RV *Tangaroa*. The ship speed was 5 knots and the swath width set to produce a consistent coverage of the seafloor with slightly overlapping edges. The data were processed with the multibeam system software package MB-System 5.0.7, taking the actual sound velocity profile gained from the CTDO casts into account. Exported xyz data were edited with Fledermaus software (Version 6.1.4b) and plotted with GMT (Wessel & Smith 1991).

Physical parameters, such as light scattering, temperature and salinity, as well as CH_4 data measured by a METS CH_4 sensor, were collected by the CTDO casts using a Seabird 911 plus system. The CTDO was deployed in two ways: in vertical casts (i.e., V04D-01) and in tow cast (i.e., T04D-01). In tow casts the CTDO is pulled c. 50 m above the seafloor at a speed of 1.5 knots. Water samples were concurrently collected in 10 litre Niskin bottles using real-time light scattering data and monitoring the voltage signal of the METS CH_4 sensor as an indication of possible higher CH_4 concentrations. The METS is a solid state sensor based on semiconductor technology and membrane separation of CH_4 (and other gases) from the water column. The sensor reacts fast (<1 min) when encountering increased CH_4 concentrations, but there is a lag-time in reaching the voltage level that represents the actual CH_4 concentrations, because gas exchange with the water column is diffusion driven. Thus, rapid changes cannot be quantitatively measured with the sensor version used in this study. As resistivity of the semiconductor depends on temperature as well, the voltage values of the CH_4 detector cannot be directly related to CH_4 concentrations, but have to be calculated using the voltage signal of the temperature detector within the METS. The final CH_4 concentrations were calculated using the calibration equation provided by the manufacturer. The METS was calibrated before the cruise, because the semiconductor drifts over time, and was kept on power 1 week before commencement of the cruise.

For gas chromatography (GC)-based CH_4 analysis, 100 ml of sea water were collected in 140 ml syringes directly from the Niskin bottles after the rosette was brought onboard. The syringes were placed in a water bath at room temperature for at least 30 min. Forty millilitres of He were added to the 100 ml of sea water and vigorously agitated for c. 2 min to reach an equilibrium between the CH_4 concentration in the water and in the gas phase. Experiments undertaken onboard and onshore determined that this method has an extraction efficiency of 88% for a 100:40 H_2O:He mixture, compared with 87% determined for a similar system at the University of Washington (unpubl. data).

The syringe head-space gas was injected directly into the GC via a drierite column to remove excess moisture. The He carrier and head-space gas used was ultra-pure grade (5 nines), and high purity was further assured by passing the He through a Valco Instruments He purifier. The sample gases were separated using a 15 m, 0.53 mm ID, 0.5 µm VP-Molesieve column and measured using a flame ionisation detector. Methane calibrations were undertaken using a range of CH_4 concentrations (0.05–5 ppm) prepared from a certified 100 ppm CH_4 standard (Scott Specialty Gases) and He (as dilutant). Measured CH_4 concentrations were corrected for extraction efficiency. A combined analytical and sampling error of c. 8% was calculated from replicate samples. Methane concentrations are reported in nanomoles per litre (nM), corrected for temperature and atmospheric pressure at the time of measurement. The lower limit of determination for dissolved CH_4 is 0.5 nM.

The hydrocarbon composition of the gas hydrate is still unknown. Pecher et al. (2004, 2005) assumed compositions to be similar to those from warm onshore seep sites (Giggenbach et al. 1993). Here, we tested to ascertain whether a pure CH_4 or mixed CH_4 and higher order hydrocarbon hydrate was more likely to be stable at Rock Garden. We calculated the geothermal gradient using the BSR depth recorded in seismic data along Line 1 across the western slope, where the BSR is clearly visible (between Common Depth Point numbers 1275 and 1375—see Fig. 3). We performed a seismic velocity analysis, determined the depth of the BSR, and calculated the pressure at the BSR, assuming hydrostatic pressure in sea water. Temperature at the BSR was predicted from gas hydrate phase boundaries using various gas compositions and the CSMHYD program (Sloan 1998). We calculated

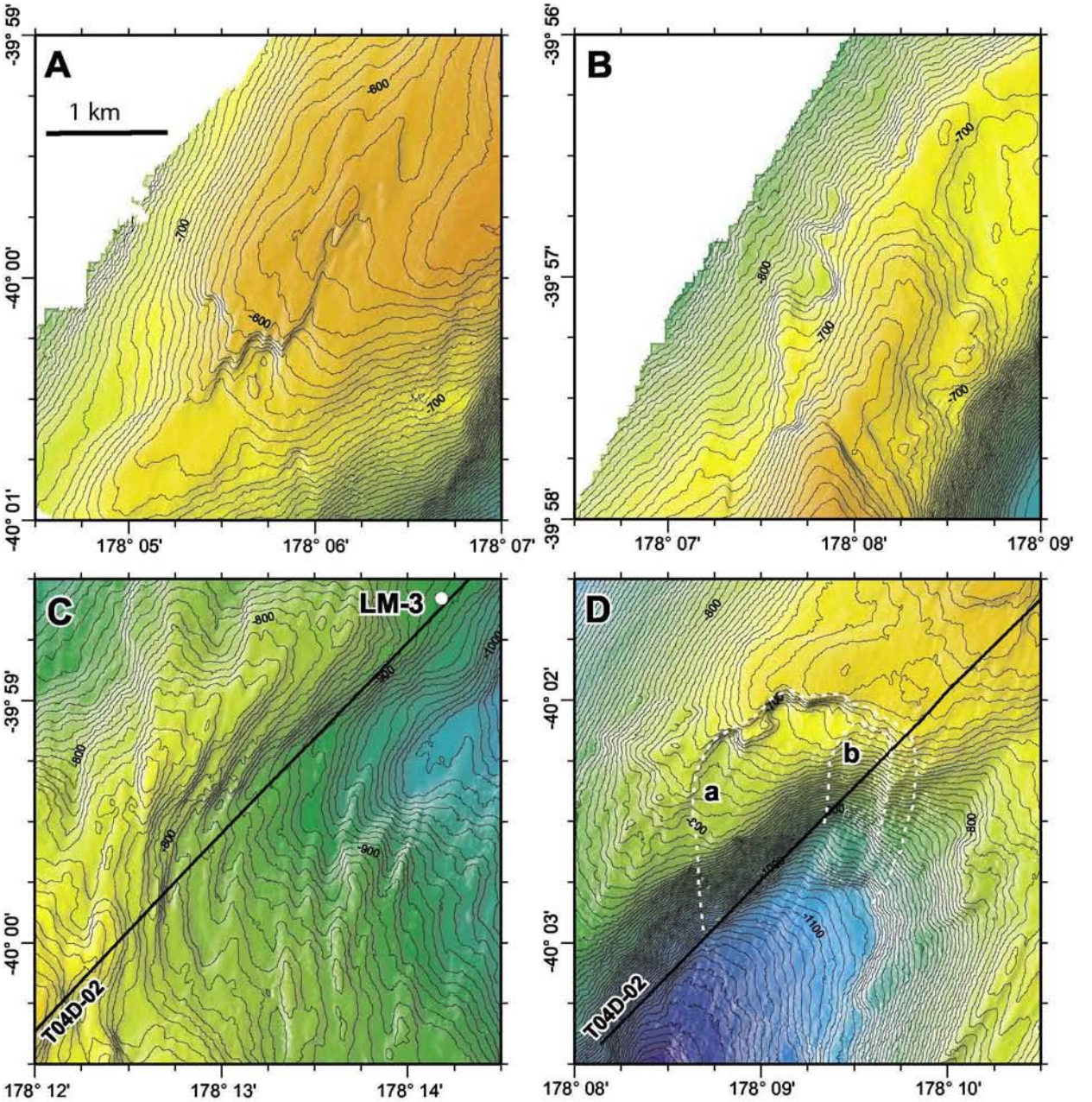

Fig. 4 Detailed bathymetry from locations marked on Fig. 2. **A**, Southern part of Western Rock Garden showing slumping structures at c. 650 mbsl. **B**, Northern part of Western Rock Garden showing slumping structures at c. 700 mbsl. **C**, Scarps with rotating strike, possibly related to the subduction of a seamount. LM-3 is the locality where a flare was observed by Lewis & Marshall (1996), close to the tow line in this study. **D**, Large slump structure in the southern part of Eastern Rock Garden; slump **a** with an upper edge depth at c. 700 mbsl is relatively older than slump **b** at c. 720 mbsl, which has re-sedimented debris at its foot.

geothermal gradients from an average temperature profile with depth shown in Pecher et al. (2005). The error margins were estimated from assuming one-quarter of a wavelength as picking error, corresponding to c. ±10 m in depth. Since the depth intervals between seafloor and BSR are relatively small (46–240 m), these picking errors are dominant compared to errors from seismic velocities. The calculated geothermal gradients were evaluated to ascertain whether a pure methane hydrate could be stable at Rock Garden.

RESULTS

New swath bathymetry

High resolution bathymetry mapping shows that Rock Garden is dominated by two prominent northeast striking ridges, called here "Eastern" and "Western" Rock Garden (Fig. 2). Western Rock Garden has a length of 17 km, width of 4.5 km and steep flanks (c. 24°) on the eastern side. The shallowest water depth (440 m) occurs on a ridge crest situated on

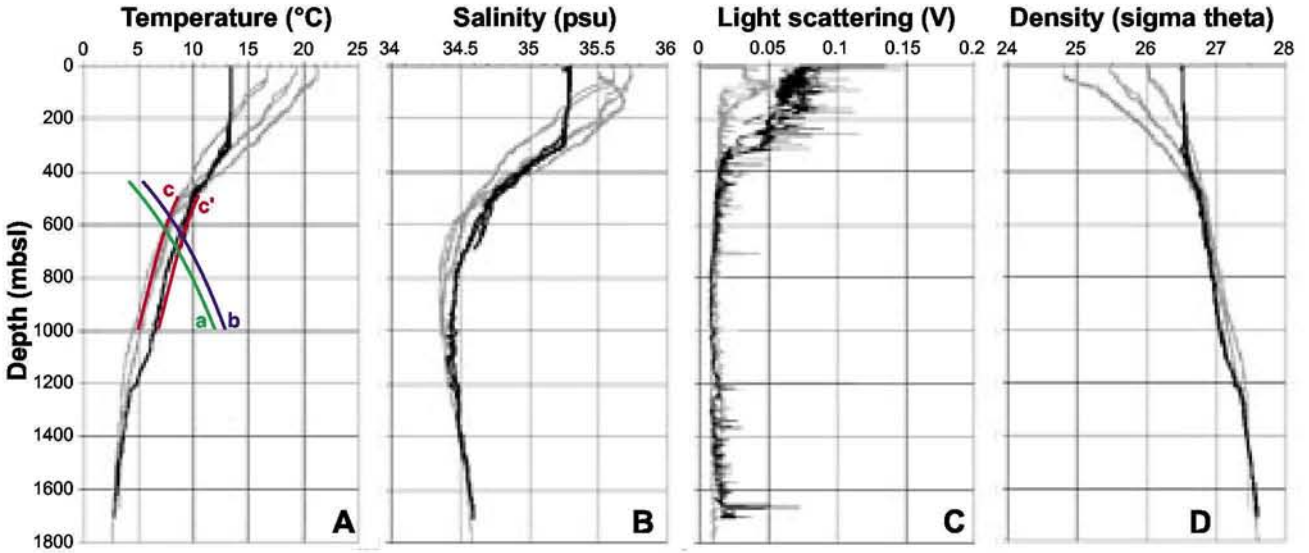

Fig. 5 Physical properties of the water column at Rock Garden (black lines) compared with the Kermadec arc (grey lines—see Fig. 1 inset). **A**, Temperature profiles: gas hydrate stability depths have been calculated for minimum (c red) and maximum (c′ red) water temperatures as reported by Pecher et al. (2005). Phase boundaries are calculated using *CSMHYD* (Sloan 1998) for pure CH_4 in sea water (green line a) and for 96.3% CH_4, 2.6% CO_2 and 1.1% ethane mole fractions (blue line b). **B**, Salinity profiles. **C**, Light scattering. **D**, Density profiles.

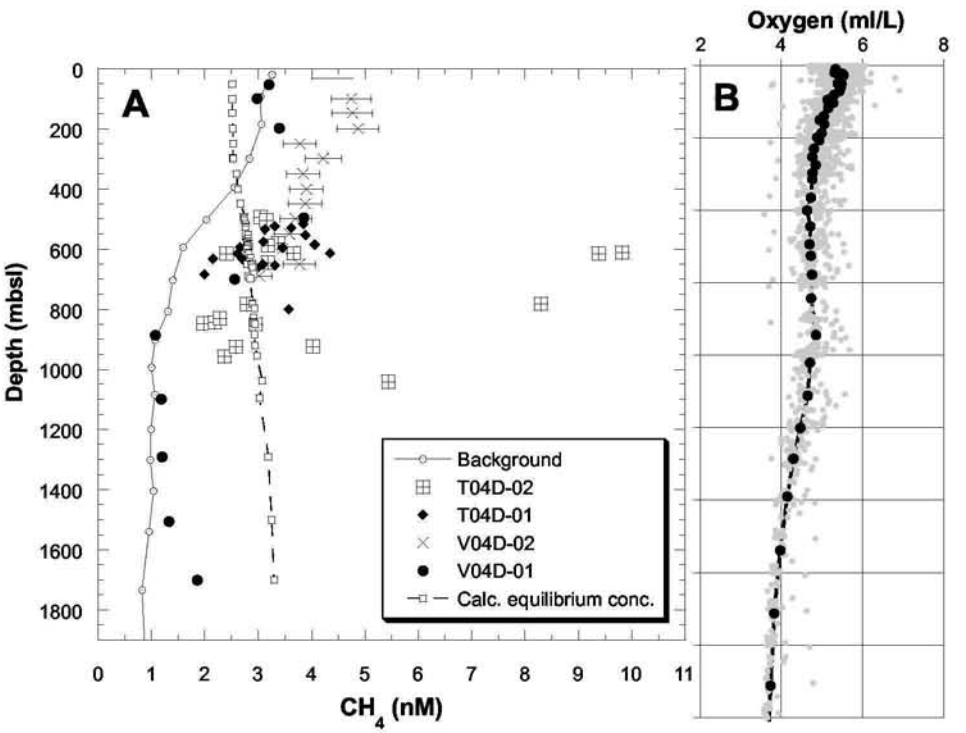

Fig. 6 **A**, Concentration of dissolved CH_4 in water samples analysed by GC. The two vertical casts (V04D-01 and V04D-02) and two tows (T04D-01 and T04D-02) from Rock Garden are compared with those from three CTD casts along the Kermadec arc. The calculated sea water CH_4 equilibrium concentrations with atmospheric methane are also plotted (Calc. equilibrium conc.). **B**, Dissolved oxygen data (black dots = av. values) from the entire east coast of New Zealand's North Island (NOAA 2005).

a plateau at c. 580 mbsl. Several smaller but steep scarps between 10 and 30 m in height can be seen on this plateau, and three large slump structures are identified on the western side of the ridge, north of the highest summit (Fig. 2, 4A,B). Eastern Rock Garden is separated from Western Rock Garden by a 2–5 km wide valley that widens towards the northeast. The valley has a northeast-striking central ridge of up to 130 m in elevation. Eastern Rock Garden is overall slightly deeper (575–790 mbsl) and flatter than Western Rock Garden, and consists of several smaller northeast-striking ridges.

In the southwest portion of Eastern Rock Garden there is a 2 km wide valley which has several large slumps (e.g., Fig. 4D). The dominant slump structures there consist of a large, relatively older structure c. 500 m northwest of the tow line (location a) and a smaller, relatively younger sediment slump feature (location b) that has debris at the foot of the slump scarp. The dominant northeast strike of ridges and structures parallel to the Hikurangi margin reflects the influence of subduction along the margin (Fig. 1). Immediately to the north of Eastern Rock Garden, curved and step-like

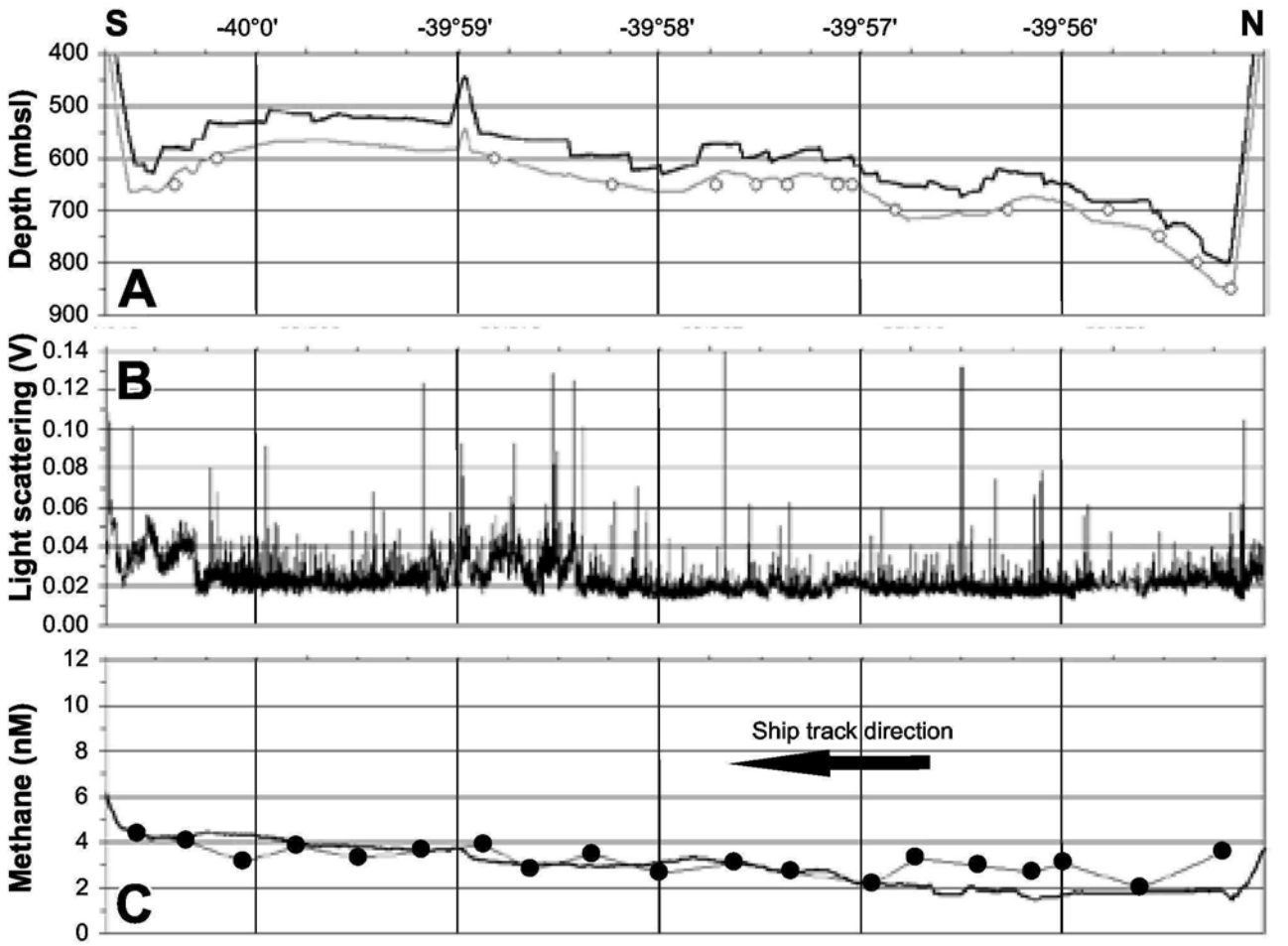

Fig. 7 Profiles of T04D-01 across Western Rock Garden. **A**, Seafloor depth (grey line) calculated from the CTD depth plus the altimeter distance and digitised depth data (open circles) from the bathymetry. **B**, Light scattering. **C**, Methane concentrations measured by METS, and GC of water samples (closed circles) collected in Niskin bottles. Combined sampling and analytical CH_4 errors for GC measurements is equal to the width of the filled circles.

structures indicate a further complicated tectonic history in this area (Fig. 4C).

Physical properties and oxygen content of the water column

Physical properties of sea water from the two vertical CTDO casts in Rock Garden and the reference stations from the Kermadec arc are shown in Fig. 5. Waters overlying Rock Garden are warmer, more saline, and slightly less dense below 300 mbsl than the Kermadec arc waters. The most obvious differences are in the near-surface waters (<300 mbsl), where the Rock Garden waters are colder and less saline, forming a well mixed upper water layer. Light scattering in the near-surface (<350 mbsl) waters is significantly higher, possibly indicating higher input of detritus from land and/or higher primary production in the study area (Fig. 5C). Sea water at depths >400 m at Rock Garden becomes increasingly more dense with depth (Fig. 5D). The density gradient will inhibit vertical mixing.

Dissolved oxygen data were not collected in this survey, but data from the entire east coast of the North Island of New Zealand (NOAA 2005) show no distinct oxygen minimum zone above 900 mbsl that may result in higher CH_4 concentrations (Fig. 6B).

Methane concentrations in the water column

Methane concentrations of sea water in cast V04D-01, c. 10 km southeast of Rock Garden (Fig. 2), are higher by 1–2 nM between 900 and 200 mbsl, compared with the background CH_4 casts obtained from the Kermadec arc at similar depths (Table 1, Fig. 6A). Below 900 mbsl and above 200 mbsl the concentrations are in good agreement with those of the Kermadec arc reference sites. V04D-02, deployed close to the area where high CH_4 concentrations had been identified during T04D-02, verifies the relatively high CH_4 concentrations between 200 and 900 mbsl. In addition, the data show increasing concentrations of CH_4 up to 5 nM with decreasing depth (Fig. 6A). Methane concentrations in the tow along Western Rock Garden (T04D-01) are similar to those obtained in the two vertical casts of the Rock Garden area, but show a variation of c. 2 nM which can not be linked to depth variations. By contrast, a clear indication for active seeping is given by four samples in T04D-02 which have concentrations up to 10 nM (Fig. 6A).

The depth profiles of the CTDO tows are shown in Fig. 7A, 8A. The seafloor depths calculated from the CTDO depth plus the altimeter distances are in good agreement with multibeam data, indicating that the CTDO-tow tracks are accurately positioned (Fig. 2). The CH_4 concentrations measured by

Table 1 Salinity, temperature, and CH_4 results from water column casts in the Rock Garden region of Ritchie Ridge. The calculated concentrations of CH_4 in equilibrium with atmosphere (1.8 ppm) are presented (equilibrium solubilities of methane from Wiesenburg & Guinasso 1979) and the percent saturation calculated.

Depth (m)	Salinity (psu)	Temperature (°C)	Methane (nM) measured	Methane (nM) in equilibrium with atmosphere	Methane saturation (%)
V04D-01: 40°5.680′S–178°17.158′E					
52	35.29	13.43	3.2	2.51	127
101	35.29	13.42	3.0	2.51	118
298	35.26	13.30	3.4	2.52	134
494	34.76	10.17	3.8	2.72	141
699	34.55	8.23	2.5	2.85	89
884	34.46	7.15	1.1	2.93	37
1096	34.44	5.86	1.2	3.03	39
1291	34.49	4.01	1.2	3.19	37
1501	34.54	3.25	1.3	3.25	41
1700	34.60	2.76	1.9	3.30	56
V04D-02: 40°2.283′S–178°9.831′E					
102	35.29	13.47	4.7	2.51	189
149	35.29	13.45	4.8	2.51	190
200	35.27	13.26	4.9	2.52	193
250	35.24	13.10	3.8	2.53	149
300	35.25	13.10	4.2	2.53	167
350	35.06	12.27	3.8	2.59	148
401	34.96	11.61	3.9	2.62	149
449	34.86	10.86	3.9	2.67	145
498	34.73	9.85	3.7	2.74	135
549	34.69	9.50	3.6	2.76	130
600	34.67	9.24	3.5	2.78	124
651	34.65	9.08	3.8	2.79	135
692	34.61	8.76	3.0	2.81	107
T04D-01: 39°54.945′S–178°10.057′E to 40°0.809′S–178°5.167′E					
797	34.50	7.19	3.6	2.93	122
683	34.53	7.56	2.0	2.91	68
649	34.54	7.65	3.1	2.89	107
631	34.57	8.10	2.7	2.86	95
662	34.55	7.76	3.0	2.89	103
654	34.57	8.01	3.3	2.87	115
630	34.57	8.05	2.1	2.86	75
593	34.60	8.45	2.7	2.84	94
574	34.64	8.85	3.1	2.81	110
613	34.61	8.57	2.6	2.83	92
594	34.65	8.83	3.5	2.81	123
566	34.64	8.77	2.8	2.81	99
553	34.65	8.80	3.9	2.81	139
528	34.70	9.32	3.6	2.77	131
524	34.71	9.35	3.3	2.77	120
517	34.70	9.45	3.8	2.76	139
534	34.72	9.59	3.1	2.76	113
583	34.62	8.50	4.1	2.83	143
612	34.62	8.53	4.3	2.83	153
T04D-02: 39°58.089′S–178°14.859′E to 40°3.406′S–178°8.182′E					
956	34.48	6.66	2.4	2.97	80
922	34.50	7.01	2.6	2.94	88
845	34.51	7.39	2.0	2.91	68
849	34.50	7.03	2.9	2.94	100
842	34.51	7.19	2.2	2.93	75
828	34.52	7.25	2.3	2.92	78
783	34.52	7.54	2.8	2.90	96
643	34.58	8.38	3.2	2.84	112
614	34.58	8.33	2.4	2.84	85
585	34.62	8.69	3.7	2.82	130
493	34.71	9.65	3.0	2.75	110
504	34.73	9.88	3.2	2.74	115
579	34.64	9.06	3.4	2.79	121
587	34.63	9.00	3.2	2.80	114
611	34.63	8.73	9.8	2.82	348
614	34.62	8.66	9.4	2.82	333
780	34.55	7.72	8.3	2.89	287
922	34.50	7.05	4.0	2.94	137
1039	34.46	5.44	5.4	3.07	177

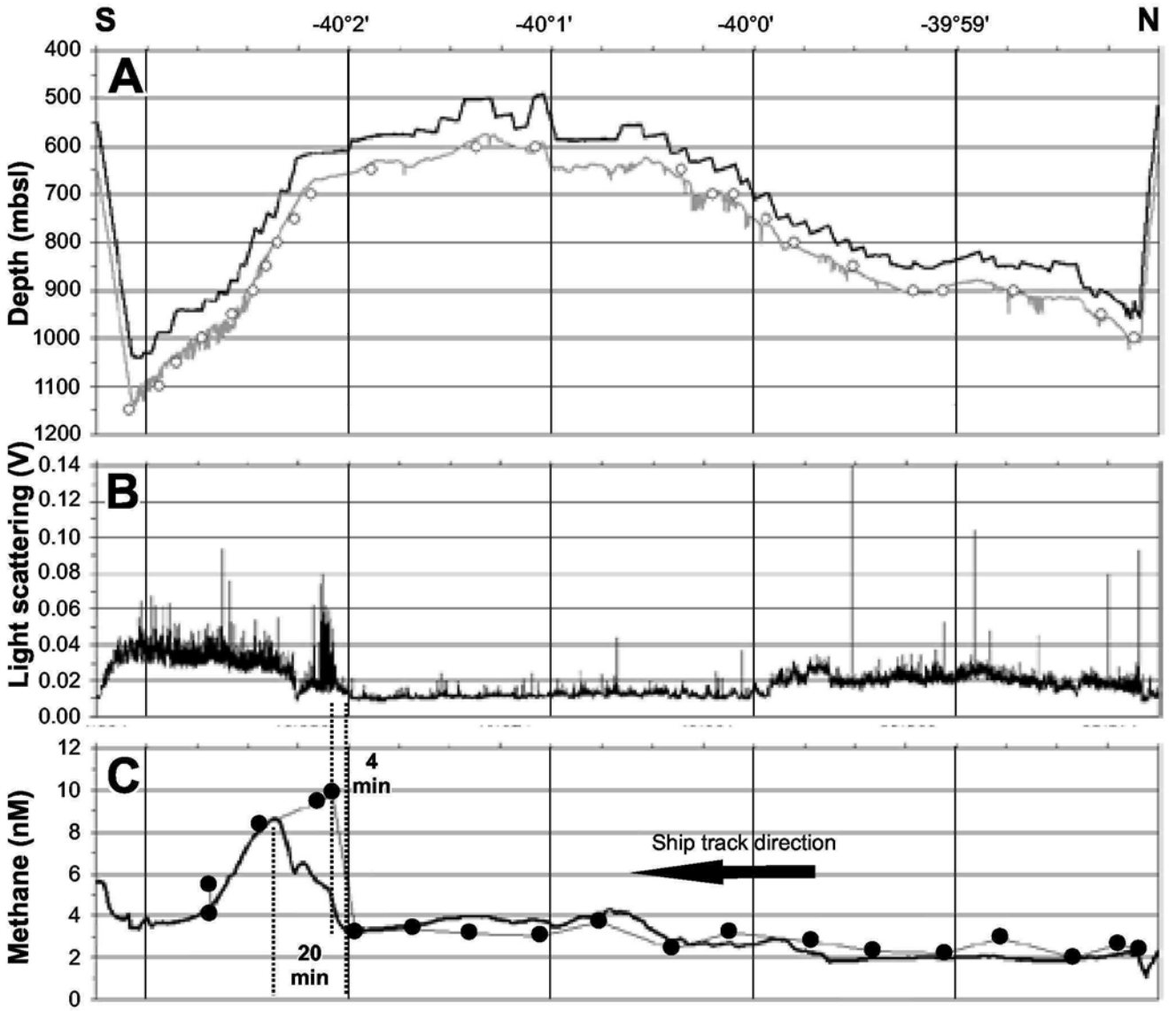

Fig. 8 Profiles of T04D-02 across Eastern Rock Garden. **A**, Seafloor depth (grey line) calculated from the CTD depth plus the altimeter distance and digitised depth data (open circles) from the bathymetry. **B**, Light scattering. **C**, Methane concentrations measured by METS, and GC of water samples (closed circles) collected in Niskin bottles. Combined sampling and analytical CH_4 errors for GC measurements are equal to the width of the filled circles.

the METS sensor are in good agreement overall with those measured by GC in discrete sea water samples (Fig. 7C, 8C). A small but perceptible increase in CH_4 concentration from north to south along both ridges is indicated. In the tow along Eastern Rock Garden (T04D-02), the METS detected elevated concentrations of CH_4 near the southwest edge of the ridge, corroborated by CH_4 analysis in the discrete water samples (Fig. 8C). However, there is an c. 20 min delay (equivalent to c. 900 m) in the METS signal, because of the time-lag for the sensor to reach its final voltage level. Nevertheless, the beginning of the CH_4 increase determined by the METS started c. 1 min before the discrete water samples with the highest CH_4 concentrations were collected. In addition, the increase in CH_4 concentration measured by the METS and the two highest CH_4 values measured in the water samples correspond to the start of elevated light scattering (Fig. 8B). The significantly higher CH_4 concentrations (between 5 and 10 nM) correspond to sea water depths between 610 and c. 1000 mbsl (Fig. 8A,C).

Flare occurrence

CTDO-tow T02D-02 was cast close to flare location LM-3 (Fig. 2) (Lewis & Marshall 1996): no geochemical or hydroacoustic indication for CH_4 release was found at the time of the survey. In contrast, a flare was observed at the location of the highest CH_4 concentrations, confirming the release of bubbles (between 40°01.980′S/178°10.018′E and 40°2.485′S/178°9.341′E). Unfortunately, the data were not recorded, and a more detailed survey could not be undertaken.

Inference of gas hydrate composition from heat flow

We have used an indirect approach to evaluate the gas hydrate composition by determining geothermal gradients from seismic

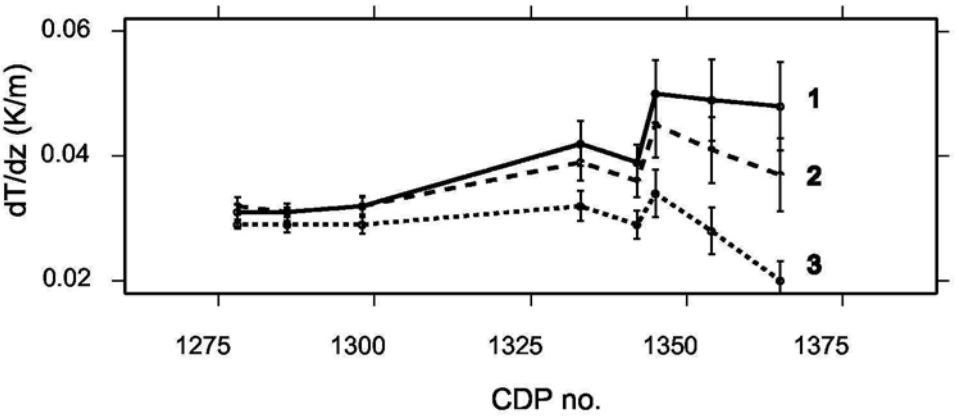

Fig. 9 The thermal gradient required to destabilise hydrates of different composition based on depths determined for BSR along seismic Line 1 (Fig. 3), western edge of Eastern Rock Garden. The gradients are calculated from phase boundaries (Sloan 1998) for gas compositions: 1. 96.0% CH_4, 2.6% CO_2, 1.1% ethane, 0.3% propane, 3.5% NaCl (Structure-II hydrate)—average of 21 onshore vents (Giggenbach et al. 1993); 2. same as 1 above, but without propane (Structure-I hydrate); and 3. methane hydrate. Errors assume one-quarter wavelength picking error. CDP no. = Common Depth Point number.

data as described above in the Methods section. Geothermal gradients from BSR depths (CDP 1275 and 1300) away from the ridge crest are c. 0.03 K/m, with values only slightly affected by the selected gas compositions (Fig. 9). Assuming pure methane hydrate (curve 3 in Fig. 9), the thermal gradient decreases towards the ridge crest. This decrease in geothermal gradient and hence heat flow towards BSR pinchouts and the ridge crest seems unrealistic. Gas hydrates are assumed to decrease sediment permeability (Kleinberg et al. 2003). Fluid flow and hence advective heat flow would be expected to be focused along the base of gas hydrates towards BSR pinchouts (i.e., towards the ridge crest). This would explain the slight increase of the thermal gradient towards the ridge crest using the phase boundary for Structure-I hydrates (CH_4-CO_2-C_2H_6; curve 2) as supposed by Pecher et al. (2005). The significantly higher geothermal gradients needed to destabilise hydrates which incorporate propane (curve 1) towards the ridge crest is caused by more stable Structure-II hydrate that will form if 0.3% propane is part of the hydrate gas composition. A decrease of thermal gradient and hence heat flow towards BSR pinchouts and the ridge crest, calculated for a pure methane hydrate (curve 3), seems unrealistic.

DISCUSSION

One of the foremost problems in studying geological, biogeochemical, and ecological processes at cold seeps is locating the active sites. Many cold seeps can be correlated with morphological structures on the seafloor, such as mud volcanoes, pockmarks, slumps, or carbonate chemoherms that form small mounds or even pinnacle-like structures (Trehu et al. 1999). The use of backscatter and side scan information obtained during multibeam surveys can locate carbonate or gas hydrate cemented areas, even though there may not be any particular morphological expression (Johnson et al. 2003; Klaucke et al. 2005; Naudts et al. 2006). Geochemical information of CH_4 anomalies and hydroacoustic data from the water column (that can detect bubbles) are the ideal combined method for locating active methane seeps at the seafloor.

Comparison of the CH_4 concentrations measured in Rock Garden with other New Zealand studies is difficult. Gas data are available from the high-temperature Calypso vent field (c. 200°C), near the volcanically active White Island, but for comparative purposes these are inappropriate because the water column has been infiltrated by CH_4 that has a volcanic source (Botz et al. 2002). The only comparison possible is with results from CTDO casts made during our expedition farther north along the Kermadec arc, in casts that were distant from known seep or high-temperature vent sites. The Kermadec arc reference sites show that, between 200 and 900 mbsl, the CH_4 concentrations are higher at Rock Garden by 1–2 nM (Fig. 6). This small but discernible increase may be due to differences in the CH_4 microbial processes because of different physical properties of the water and/or the proximity of the Rock Garden area to land (Fig. 1). But, it may also reflect a higher background CH_4 concentration because of widespread focused or diffuse CH_4 seepage. This possibility is supported by the observed increase from north to south along both tows over Western and Eastern Rock Garden (Fig. 7C, 8C, 10). However, more detailed research is required to confirm whether this is a local phenomenon linked to seepage or whether it reflects the typical CH_4 distribution along the Hikurangi margin caused by unknown processes.

Calculated CH_4 values of sea water in equilibrium with air (c. 1.8 ppm CH_4) at various depths are presented in Table 1 and plotted on Fig. 6A. The CH_4 concentration of the water above c. 600 m is typically oversaturated (mostly 120–150%) and undersaturated below this depth (down to 35%). Deeper mid-water column samples usually are undersaturated due to microbial oxidation and mixing with older deeper water that last equilibrated at the sea surface with an atmosphere that had lower CH_4 concentrations. Samples collected in T04D-02 (1050–600 m) clearly have surplus CH_4 (up 350% of atmosphere equilibrated sea water) that can not be accounted for by normal oceanographic processes (Table 1, Fig. 6A). The two water samples with the highest CH_4 values (>8 nM; Fig. 8) in T04D-02 indicate a localised methane source at the edge of the Eastern Rock Garden plateau at 660 mbsl, near the headwall of the slump structures and the location of the observed flare. The two water samples were collected because of the distinct increase of light scattering which, in hydrothermal surveys, is commonly used as an indicator of active venting. In hydrothermal systems, elevated light scattering is caused by mineral precipitates in the water column, which is unlikely to be the case at Rock Garden. However, fluids and/or bubbles may transport fine-grained sediment in the water column, or simple erosion may be taking place at the edge of the plateau

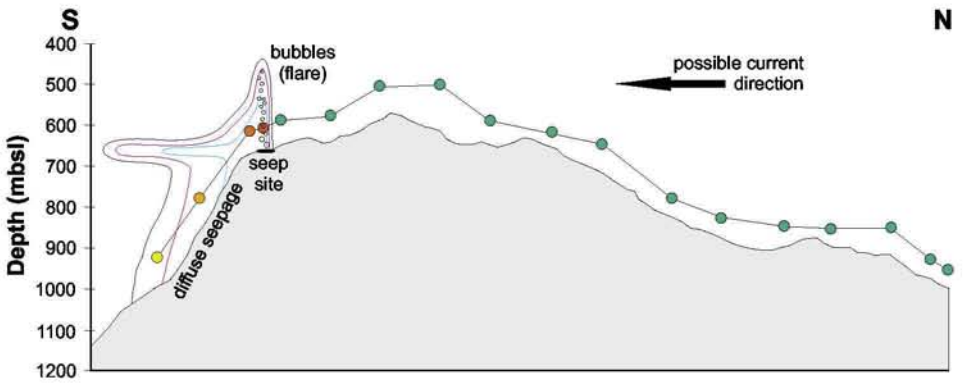

Fig. 10 Schematic diagram showing the CH_4 concentrations measured in discrete water samples in T04D-02 along Eastern Rock Garden. The locality of the seep position and possible distribution of CH_4 in the water column is based on data and observations. Green dots <4 nM, red dots c. 10 nM, orange dot c. 8 nM, and yellow dot c. 6 nM.

and particulate matter is transported into the water column. It may be that the erosion is higher because of weakening of the sediments due to fluid seepage which enhances sediment erosion. The possibility that the light scattering sensor detected bubbles is unlikely, or just coincidental, as the METS sensor showed increasing CH_4 values c. 4 min before the increase in light scattering (Fig. 8B,C).

Based on our data and observations we suggest that the significant CH_4 anomaly at the southwest plateau edge of Eastern Rock Garden is driven by the release of dissolved as well as free CH_4. The sea water has a density gradient at depths below 400 m (Fig. 5D), so it is likely that most of the dissolved methane released at seep sites, or as diffuse flux from large areas, is horizontally distributed by currents (Fig. 10). Seep fluids, which may be slightly less dense than the bottom water in which they are released, could be laterally distributed slightly higher up in the water column where the density is the same as that of the fluid. Methane from a diffuse source is probably transported along the same depth interval as the source itself. Gas bubbles are expected to rise rapidly in the water column (c. 25 cm/s for millimetre sized bubbles) and undergo a relatively rapid dissolution and gas stripping into the surrounding water (e.g., Leifer & Patro 2002). Bubble-released methane will form a vertical plume-shaped methane distribution, with the highest methane concentrations close to the seafloor, which is then distributed horizontally by currents (Fig. 10). It is highly possible that a vertical injection of methane into the water column was occurring at Eastern Rock Garden at the time of sampling because bubbles were detected by the ship's echosounder. The detection of a flare and its coincidence with the highest methane measurements most probably suggests that the two highest methane concentrations are caused as a consequence of dissolution of bubble-transported methane. Two samples collected before the one with the highest CH_4 concentrations (10 nM) were obtained in similar water depths (c. 600 m) but had CH_4 concentrations of c. 3 nM. This means that a focused methane source exists, which, as indicated by the observed flare, released methane bubbles that dissolved and were distributed by southward-directed currents (Chiswell 2005) (Fig. 10). High CH_4 concentrations have been detected down to c. 1000 mbsl during tow T04D-02. The elevated CH_4 concentrations at the southern end of this tow may reflect additional localised seepage within the slump areas or a more widespread CH_4 release from CH_4-rich sediments that have been exhumed due to the slumping process, releasing diffuse methane into the water column. Because of the density gradient, it is unrealistic that methane released at c. 670 mbsl is distributed downward to this depth.

The lack of a methane anomaly at the vent site (LM3) described by Lewis & Marshall (1996) may be explained by the ephemeral nature of seep activity (Heeschen et al. 2005; Greinert et al. 2006). Alternatively, in the past decade, supply of methane through gas conduits into the seep site, as imaged by seismic data (Pecher et al. 2004), might have changed and the gas is being released to the seafloor elsewhere.

The seafloor depth in the area of highest methane concentrations (c. 670 mbsl) is very close to the depth of BSR pinchouts at c. 630 mbsl (Fig. 3). This roughly marks the long-term (longer than water temperature fluctuations) top of gas hydrate stability at Rock Garden (note: this observation is independent of the assumed phase boundary). Despite the uncertainty of the gas hydrate composition, we speculate that methane release is strongly linked to gas hydrate zone pinch outs, either because of decomposing gas hydrate or due to free gas that migrates beneath the base of a lower permeability hydrate zone towards the seafloor.

The top of the headwall of the slumps (Fig. 4D) coincides roughly with the top of the gas hydrate stability zone, similar to that observed in seismic data (Pecher et al. 2005). Our bathymetric data therefore support the proposed model of slumping following depressurisation during uplift leading to dissociation of gas hydrate at the base of gas hydrate stability, generation of free gas, pore volume expansion, overpressure, and sediment weakening. After slumping, gas would be expected to be released from the base of gas hydrate stability. Whether gas hydrate decomposition directly causes higher CH_4 concentration and subsequent seafloor slumping is presently unproven. Nevertheless, because of the prominent BSR structures in the Rock Garden area, we infer that gas hydrates are a significant, if not a controlling factor for seepage and seafloor stability along the Hikurangi margin.

SUMMARY

A multibeam survey of the Rock Garden region has shown that it consists of two prominent, northeast-trending ridges and that slumping is common along the slopes of the ridges. The ridges and large-scale structures are parallel to subduction along the Hikurangi margin. A survey of the Rock Garden site shows relatively elevated concentrations of CH_4 (up to 10× background) in the water column. The anomalous CH_4 concentrations are associated with a comparatively young

slump structure in the southern end of the Eastern Rock Garden ridge. The depth (610 mbsl) of maximum CH_4 concentration and the plateau itself are close to the depth where BSR's pinch out at the seafloor surface. Relatively high CH_4 concentrations are measured down to depths of 1000 mbsl, most likely as a consequence of sediment slumping induced by gas hydrate destabilisation and/or marking seepage through the gas hydrate zone. Methane concentrations calculated from data collected by a METS sensor attached to a CTDO, and concentrations measured by GC in sea water samples, are in good agreement and indicate focused CH_4 release. No elevated CH_4 concentrations were measured in the northern part of Eastern Rock Garden where a flare, visible on fish finding sonar, was previously described by Lewis & Marshall (1996), underlining the ephemeral nature of CH_4 seeps in general.

ACKNOWLEDGMENTS

The research was supported by the CRI Capability Funding, the New Zealand Foundation for Research, Science and Technology contracts C05X0406 (GNS Science) and C01X0203 (NIWA), and the NOAA Vents Program. We thank officers and crew of the RV *Tangaroa* for their assistance during the cruise. Jens Greinert thanks the EU for funding his work through the Marie Curie grant MOIF-CT-2005-007436.

REFERENCES

Boetius A, Ravenschlag K, Schubert CJ, Rickert D, Widdel F, Gieseke A, Amann R, Jorgensen BB, Witte U, Pfannkuche O 2000. A marine microbial consortium apparently mediating anaerobic oxidation of methane. Nature 407(6804): 623–626.

Bohrmann G, Ivanov M, Foucher J-P, Spiess V, Bialas J, Greinert J, Weinrebe W, Abegg F, Aloisi G, Artemov Y and others 2003. Mud volcanoes and gas hydrates in the Black Sea: new data from Dvurechenskii and Odessa mud volcanoes. Geo-Marine Letters 23: 239–249.

Borowski WS, Paull CK, Ussler WUI 1997. Carbon cycling within the upper methanogenic zone of continental rise sediments: an example from the methane-rich sediments overlying the Blake Ridge gas hydrate deposits. Marine Chemistry 57: 299–311.

Botz R, Wehner H, Schmitt M, Worthington TJ, Schmidt M, Stoffers P 2002. Thermogenic hydrocarbons from the offshore Calypso hydrothermal field, Bay of Plenty, New Zealand. Chemical Geology 186(3–4): 235–248.

Buffett B, Archer D 2004. Global inventory of methane clathrate: sensitivity to changes in the deep ocean. Earth and Planetary Science Letters 227(3–4): 185–199.

Chiswell SM 2005. Mean and variability in the Wairarapa and Hikurangi eddies. New Zealand Journal of Marine and Freshwater Research 39: 121–134.

Collett TS, Kuuskraa VA 1998. Hydrates contain vast store of world gas resources. Oil and Gas Journal 96(19): 90–95.

Field BD, Uruski CI, Beu A, Browne G, Crampton J, Funnell R, Killops S, Laird M, Mazengarb C, Morgans H and others 1997. Cretaceous-Cenozoic geology and petroleum systems of the east coast region, New Zealand. Lower Hutt, New Zealand, Institute of Geological & Nuclear Sciences. 301 p.

Giggenbach WF, Stewart MK, Sano Y, Goguel RL, Lyon GL 1993. Isotopic and chemical composition of the waters and gases from the East Coast accretionary prism, New Zealand. Philippines, Dumaguete. Pp. 208–231.

Greinert J, Gerhard B, Suess E 2001. Gas hydrate-associated carbonates and methane-venting at Hydrate Ridge: classification, distribution and origin of authigenic lithologies. In: Paull CK, Dillon WP ed. Natural gas hydrates: occurrence, distribution and detection: American Geophysical Union Geophysical Monograph 124: 99–113.

Greinert J, Artemov Y, Egorov V, De Batist M, McGinnis D 2006. 1300-m-high rising bubbles from mud volcanoes at 2080 m in the Black Sea: hydroacoustic characteristics and temporal variability. Earth and Planetary Science Letters 244(1–2): 1–15.

Heeschen KU, Collier RW, de Angelis MA, Suess E, Rehder G, Linke P, Klinkhammer GP 2005. Methane sources, distributions, and fluxes from cold vent sites at Hydrate Ridge, Cascadia Margin. Global Biogeochemical Cycles 19(2): doi:10.1029/2004GB002266.

Henrys SA, Ellis S, Uruski C 2003. Conductive heat flow variations from bottom-simulating reflectors on the Hikurangi margin, New Zealand. Geophysical Research Letters 30: 1065–1068.

Johnson JE, Goldfinger C, Suess E 2003. Geophysical constraints on the surface distribution of authigenic carbonates across the Hydrate Ridge region, Cascadia margin. Marine Geology 202: 79–120.

Jørgensen NO 1992. Methane-derived carbonate cementation of marine sediments from the Kattegat, Denmark: geochemical and geological evidence. Marine Geology 103: 1–13.

Katz HR 1982. Evidence of gas hydrates beneath the continental slope, East Coast, North Island, New Zealand. New Zealand Journal of Geology and Geophysics 25: 193–199.

Klaucke I, Sahling H, Bürk D, Einrebe WW, Ohrmann GB 2005. Mapping deep-water gas emissions with sidescan sonar. EOS 86(38): 341–344.

Kleinberg RL, Flaum C, Griffin DD, Brewer PG, Malby GE, Peltzer ET, Yesinowski JP 2003. Methane hydrate growth habit in porous media and its relationship to hydraulic permeability, deposit accumulation, and submarine slope stability. Journal of Geophysical Research. 108(2508): doi:10.1029/2003JB002389.

Kulm LD, Suess E, Moore JC, Carson B, Lewis BT, Ritger SD, Kadko DC, Thornburg TM, Embley RW, Rugh WD and others 1986. Oregon subduction zone: venting fauna and carbonates. Science 231: 561–566.

Kvenvolden KA 1988. Methane hydrate—a major reservoir of carbon in the shallow geosphere? Chemical Geology 71(1–3): 41–51.

Kvenvolden KA 1993. Gas hydrates—geologic perspective and global change. Reviews of Geophysics and Space Physics 31: 173–187.

Kvenvolden KA 1998. A primer on the geological occurrence of gas hydrate. In: Henriet J-P, Mienert J ed. Gas hydrates: relevance to world margin stability and climate change: Geological Society. Pp. 9–30.

Leifer I, Patro RK 2002. The bubble mechanism for methane transport from the shallow sea bed to the surface: a review and sensitivity study. Continental Shelf Research 22(16): 2409–2428.

Lewis KB, Marshall BA 1996. Seep faunas and other indicators of methane-rich dewatering on New Zealand convergent margins. New Zealand Journal of Geology and Geophysics 39: 181–200.

Lilley MD, Feely RA, Trefry JH 1995. Chemical and biological transformations in hydrothermal plumes. In: Humphris SE, Zierenberg RA, Mulineaux LS, Thomson RE ed. Sea floor hydrothermal systems: physical, chemical, biological, and geological interactions. American Geophysical Union Geophysical Monograph 91: 369–391.

Milkov AV 2005. Molecular and stable isotope compositions of natural gas hydrates: a revised global dataset and basic interpretations in the context of geological settings. Organic Geochemistry 36(5): 681–702.

Naudts L, Greinert J, Artemov Y, Staelens P, Poort J, Van Rensbergen P, De Batist M 2006. Geological and morphological setting of 2778 methane seeps in the Dnepr paleo-delta, northwestern Black Sea. Marine Geology 227(3–4): 177.

Nauhaus K, Boetius A, Krüger M, Widdel F 2002. In vitro demonstration of anaerobic oxidation of methane coupled to sulphate reduction in sediment from a marine gas hydrate area. Environmental Microbiology 4: 296–305.

NOAA 2005. World ocean data base. http://www.nodc.noaa.gov/OC5/southeastLECT/dbsearch/dbsearch.html [accessed September 2005].

Orpin AR 1997. Dolomite chimneys as possible evidence of coastal fluid expulsion, uppermost Otago continental slope, southern New Zealand. Marine Geology 138: 51–67.

Paull CK, Ill WU, Borowski WS, Spiess FN 1995. Methane-rich plumes on the Carolina continental rise: associations with gas hydrates. Geology 23: 89–92.

Pecher IA, Henrys SA, Bannister S, Davey F, Nishimura Y, Yamada A, Shimamura H 2003. Structure of the Hikurangi subduction zone, East Coast New Zealand, from a coincident ocean bottom seismometer, onshore/offshore, and multichannel seismic reflection survey. In: Seismic 2003. International Symposium on Deep Seismic Profiling of the Continents and their Margins, Taupo, New Zealand. Wellington, Institute of Geological and Nuclear Sciences. P. 110.

Pecher IA, Henrys SA, Zhu H 2004. Seismic images of gas conduits beneath vents and gas hydrates on Ritchie Ridge, Hikurangi margin, New Zealand. New Zealand Journal of Geology and Geophysics 47: 275–279.

Pecher IA, Ellis S, Henrys SA, Chiswell SM, Kukowski N 2005. Erosion of the seafloor at the top of the gas hydrate stability zone on the Hikurangi margin, New Zealand. Geophysical Research Letters 32(L24603): doi:10.1029/2005GL024687.

Reeburgh WS 1996. "Soft spots" in the global methane budget. In: Lidstrom ME, Tabita FR ed. Microbial growth on C1 compounds. Norwell, MA, Kluwer Academic Publishers. Pp. 334–342.

Ritger S, Carson B, Suess E 1987. Methane-derived authigenic carbonates formed by subduction-induced pore-water expulsion along the Oregon/Washington margin. Geological Society of America Bulletin 98(2): 147–156.

Sloan ED 1998. Clathrate hydrates of natural gases. New York, Dekker.

Sommer S, Pfannkuche O, Linke P, Luff R, Greinert J, Drews M, Gubsch S, Pieper M, Poser M, Viergutz T 2006. The efficiency of the benthic filter—biological control of the emission of dissolved methane from sediments hosting shallow gas hydrates at Hydrate Ridge 2. Global Biogeochemical Cycles 20: GB2019, doi:10.1029/2004GB002389.

Suess E, Torres ME, Bohrmann G, Collier RW, Greinert J, Linke P, Rehder G, Trehu A, Wallmann K, Winckler G and others 1999. Gas hydrate destabilization: enhanced dewatering, benthic material turnover and large methane plumes at the Cascadia convergent margin. Earth and Planetary Science Letters 170(1–2): 1–15.

Townend J 1997. Estimates of conductive heat flow through bottom-simulating reflectors on the Hikurangi margin and southwest Fiordland, New Zealand. Marine Geology 141: 209–220.

Trehu AM, Torres ME, Moore GF, Suess E, Bohrmann G 1999. Temporal and spatial evolution of a gas hydrate-bearing accretionary ridge on the Oregon continental margin. Geology 27(10): 939–942.

Treude T, Boetius A, Knittel K, Wallmann K, Jorgensen BB 2003. Anaerobic oxidation of methane above gas hydrates at Hydrate Ridge, NE Pacific Ocean. Marine Ecology Progress Series 264: 1–14.

Wessel P, Smith WHF 1991. Free software helps map and display data. EOS Transactions AGU 72: 445–446.

Whiticar MJ 1999. Carbon and hydrogen isotope systematics of bacterial formation and oxidation of methane. Chemical Geology 161(1–3): 291–314.

Wiesenburg DA, Guinasso NL 1979. Equilibrium solubilities of methane, carbon monoxide, and hydrogen in water and sea water. Journal of Chemical Engineering Data 24: 356–360.